Geophys. J. Int. (1999) **136,** 373–384

Anisotropy of heterogeneity scale lengths in the lower mantle from *PKIKP* precursors

Vernon F. Cormier

Department of Geology and Geophysics, University of Connecticut, Storrs, CT06269–2045, *USA. E-mail: cormier@geol.uconn.edu*

Accepted 1998 August 28. Received 1998 July 3; in original form 1998 January 25

SUMMARY

The anisotropy of heterogeneity scale lengths in the lower mantle is investigated by modelling its effect on the high-frequency precursors of *PKIKP* scattered by the heterogeneities. Although models having either an isotropic or an anisotropic distribution of scale lengths can fit the observed coda shapes of short-period precursors, the frequency content of broad-band *PKIKP* precursors favours a dominantly isotropic distribution of scale lengths. Precursor coda shapes are consistent with 1 per cent fluctuations in *P* velocity in the wavenumber band 0.05–0.5 km^{-1} extending to 1000 km above the core–mantle boundary, and with a D″ region open to circulation throughout the lower mantle. The level of excitation of *PKIKP* precursors observed in the frequency band 0.02–2 Hz requires a power spectrum of heterogeneity that is nearly white or slowly increasing with wavenumber. Anisotropy of scale lengths may exist in a D″ layer having larger horizontal than vertical scale lengths and produce little or no detectable effects on *PKIKP* precursors for *P*-velocity perturbations as high as 3 per cent when averaged over a vertical scale of several kilometres, and much higher when averaged over scales of hundreds of metres or less.

Key words: core–mantle boundary, mantle heterogeneity, scattering.

1 INTRODUCTION

1.1 Precursors to *PKIKP*

A high-frequency precursor to *PKIKP* is often observed in the 130°–140° range. It is best observed on short-period instruments from sources enriched in high frequency, such as deep-focus earthquakes, in which *P* rays traverse the upper-mantle low-*Q* zone just once, or explosions, which have a higher corner frequency than earthquakes of equivalent moment. When recordings in broad-band and short-period (or long-period and short-period) pass bands are compared, the arrival of the high-frequency scattered precursor can be easily distinguished from the diffraction from the *PKP*-B caustic by its quite different frequency content and arrival time (e.g. Fig. 1). The pioneering work of Cleary & Haddon (1972) showed that the high-frequency precursors are best explained in arrival time and slowness distribution by the scattering of *P* waves by topography on the core–mantle boundary and by heterogeneities in the lower 200 km of the mantle. The location and character of these heterogeneities are recognized to be important in geodynamic models of slab cycling, plume formation and chemical heterogeneity of the lower and mid-mantle.

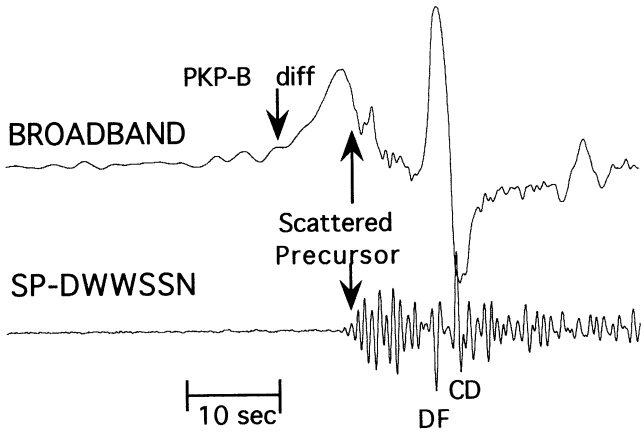

Figure 1. Example data showing broad-band and short-period waveforms near 140° (station MCWV at 139.6° from a 498-km-deep event in the Banda Sea). Note that the arrival time of the short-period precursor to *PKIKP* is later than the onset of the long-period diffraction from the *PKP*-B caustic.

1.2 Observations of heterogeneity in the lowermost mantle

Many other observations, in addition to *PKIKP* precursors (Doornbos 1976, 1988; Bataille & Flatte 1988), suggest

increased heterogeneity in the lower mantle, particularly the lowermost 250 km (Bullen's D″). The diversity and varying sensitivity of different data have complicated the search for a simple description of lower-mantle structure. Important constraints from body waves over a broad band of frequencies include wide-angle reflections from discontinuities within D″ (Lay & Helmberger 1983; Weber & Davis 1990; Kendall & Shearer 1994), waveforms and decay rates of diffracted *P* waves (Wysession *et al.* 1992; Souriau & Poupinet 1993), differential traveltimes of diffracted *P* and *SmKS* waves (Wysession *et al.* 1995; Sylvander & Souriau 1996), particle motions and anisotropy inferred from long-period *S* waves (Maupin 1994; Vinnik *et al.* 1995; Kendall & Silver 1996; Matzel *et al.* 1996; Garnero & Lay 1997), and observations of short-period *P* well beyond the core shadow (Bataille *et al.* 1990; Bataille & Lund 1996). Each of these types of wavefields samples the lower mantle at either a different incidence angle, a different time interval of interaction, a different scale length of spatial averaging, or a different level of sensitivity to elastic moduli or density variations. Although this paper concentrates on an aspect of lower-mantle heterogeneity that primarily affects the scattered precursors to *PKIKP*, discussions of experimental results will attempt to predict, where appropriate, features of heterogeneity that will affect other body-wave data.

1.3 Objectives

The primary goal of this paper is to expand the type of statistical model of heterogeneity considered in previous studies of *PKIKP* precursors, specifically to examine the effects of heterogeneity having much longer scale lengths in one or two coordinate directions. The effects of such structures have been considered in studies of other types of wavefields, but not yet considered in studies of *PKIKP* precursors. Are high-frequency *PKIKP* precursors also sensitive to the structures determined from very different types of data? Examples include *S* data consistent with either transverse isotropy in D″ or ultra-low-velocity zones at the core–mantle boundary. Sensitivity of these structures to very different types of wavefields may help to constrain the shape and scale lengths of heterogeneity in the lower mantle.

The recent study of *PKIKP* precursors by Hedlin *et al.* (1997) found that small-scale (8 km) heterogeneity persists up to 1000 km above the core–mantle boundary at a relatively uniform perturbation of 1–2 per cent in *P* velocity. This finding has important geodynamic significance, consistent with mantle circulation extending from the core–mantle boundary to mid-mantle depths. Hedlin *et al.*'s study, in common with many previous studies of *PKIKP* precursors, assumed the validity of ray theory for incident and scattered wavefields. A secondary goal in this paper is to check the accuracy of Hedlin *et al.*'s result with a calculation that incorporates frequency-dependent diffraction effects from the caustic surface in the outer core.

1.4 Modelling methods

The *PKIKP* precursor modelling algorithm described in Cormier (1995) (hereinafter referred to as Paper I), based on 3-D distributions of spheres embedded in the background medium, is extended to continuous heterogeneity described statistically. The technique assumes single scattering, but is not restricted to weak perturbations of the medium, and includes scattering into the B caustic as well as inner-core branches, and the diffracted extension of the B caustic to shorter distances. Details of the extension of Paper I, including model construction, are given in the Appendix.

2 COMPUTATIONAL EXPERIMENTS

2.1 Isotropic scale lengths

Heterogeneous models of the lower mantle were constructed using the methods described by Frankel & Clayton (1986). First, an isotropic model (Fig. 2) was assumed with a Gaussian autocorrelation with a constant correlation length in all three orthogonal directions. The fundamental scale length, percentage perturbation from the background *P* velocity, and thickness of the heterogeneous region above the core–mantle boundary were varied to fit the amplitude and shape of stacked coda of *PKIKP* precursors processed by Hedlin *et al.* (1997).

Fig. 3 shows a synthetic record section of scattered precursors and *PKIKP* waveforms observed on a short-period WWSSN instrument for a best-fitting model to the stacked precursor coda. Under the assumptions of the scattering theory used, the traveltimes of the direct, unscattered phases are unaffected by the weak perturbations of the background model, which are assumed to average to zero over the Fresnel zones of the direct phases. Note in Fig. 3 that the amplitude of precursor coda increases as the range approaches the B caustic, behaviour seen in record sections of data. Data near 140° have a high precursor to direct *PKIKP* amplitude ratio and give the strongest constraints on the model of heterogeneity.

Fig. 4 summarizes the results of experiments in which parameters characterizing an isotropically heterogeneous model were

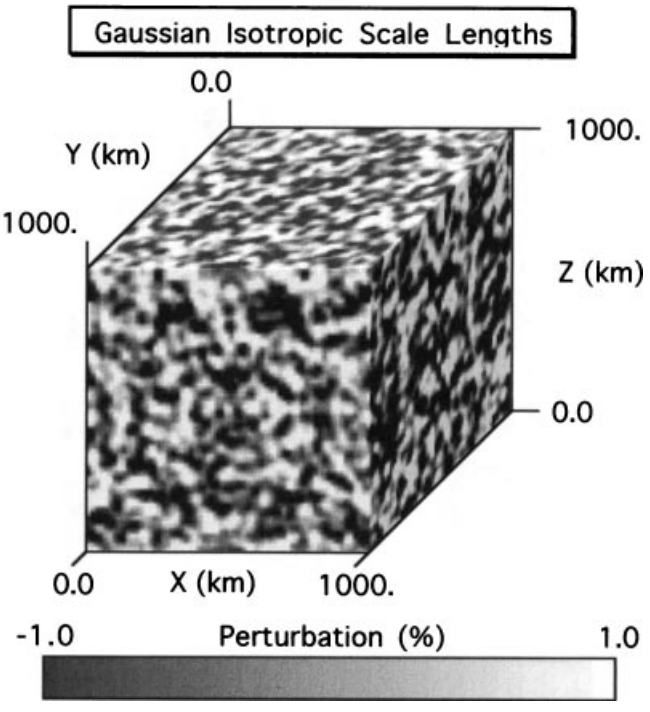

Figure 2. Isotropic heterogeneity at the base of the mantle (model I.1000). A Gaussian autocorrelation is assumed with equal correlation lengths in three orthogonal directions. A 1 per cent perturbation in the standard deviation of the *P* velocity is assumed.

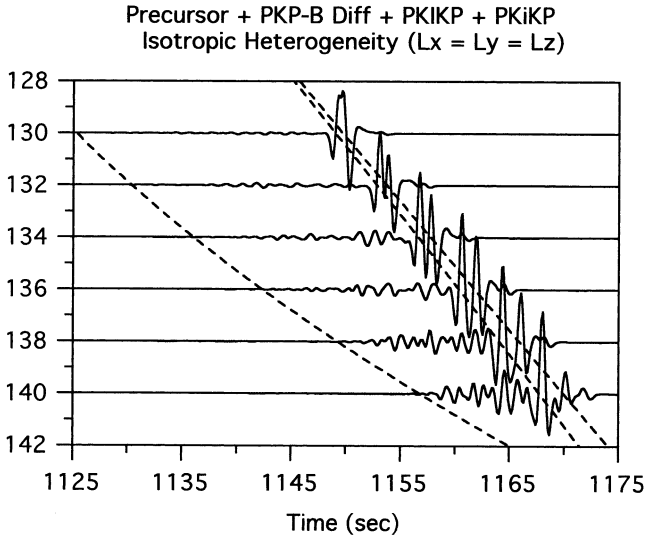

Figure 3. Synthetic record section of $PKIKP + PKiKP +$ scattered precursors for the model I.1000 shown in Fig. 2. The vertical component of displacement is shown for a WWSSN instrument response due to an explosive point source at the surface. The 1 Hz PREM (Dziewonski & Anderson 1981) is assumed for velocities, densities and attenuation. A continental crust is substituted for the crustal layers of PREM, which include a global average water layer. The heterogeneous perturbation from PREM consists of 100 m maximum topography of the core–mantle boundary with 20 km Gaussian autocorrelation lengths in horizontal directions and a 1000-km-thick layer of 1 per cent perturbations in P velocity with 20 km scale lengths in three orthogonal directions. The arrival time for precursors scattered from the core–mantle boundary is dashed.

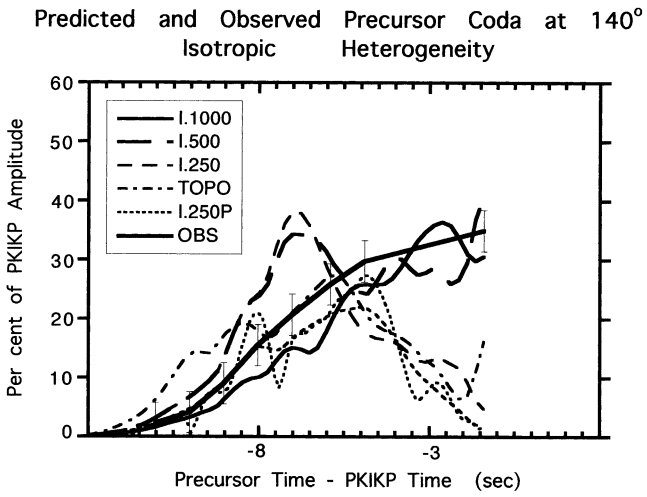

Figure 4. Predicted and observed scattered coda for different heights of heterogeneity with isotropic scale lengths. Observed coda amplitudes at 140° are from Hedlin *et al.* (1997). Predicted coda amplitudes are obtained from smoothed envelopes. All heterogeneous models, except TOPO, include 100 m of core–mantle topography with a 20 km correlation length in the horizontal directions. The best fit to observations is obtained with model I.1000, which has a 1 per cent perturbation in P velocity extending 1000 km above the core–mantle boundary. Other models tested include the following: I.500, a 500-km-thick D″ of 1.5 per cent heterogeneity; I.250 and I.250P, a 250-km-thick D″ of 1.9 per cent heterogeneity using a Gaussian and a power-law heterospectrum, respectively; and TOPO, a model of no mantle heterogeneity but with core–mantle topography with a peak amplitude of 4.7 km.

varied to fit the amplitude and shape of the precursor coda at 140°. The results agree well with those obtained by Hedlin *et al.* (1997). Only models having heterogeneity extending to 1000 km above the core–mantle boundary can fit the shape of the late coda. The intensity of perturbation for models that fix heterogeneity to a thinner D″-type layer of 250–500 km thickness must be 2–3 per cent to fit the early part of the precursor coda, but all of these models fail to fit the later part of the coda. Assuming a deep-focus source and the PREM Q model, the best-fitting model has heterogeneity uniformly extending up to 1000 km above the core–mantle boundary. The best-fitting intensity of perturbation (1 per cent) in the lower mantle may vary by up to a factor of 2 higher or lower depending on the Q model assumed and the depth of the source. In order to obtain a good fit to apparent arrival times of the precursor coda, the heterogeneity must begin immediately at the core–mantle boundary. Core–mantle boundary topography is adjusted to be consistent with inferred density perturbations and constrained not to produce observable effects on PcP (e.g. Menke 1986). This results in CMB topography having horizontal correlation lengths of the order of 20 km with a maximum height of 100 m.

2.2 Anisotropic scale lengths

2.2.1 Large horizontal scale/small vertical scale

Long horizontal scale lengths of heterogeneity in D″ may be consistent with observations of reflections of P and S waves observed from either discontinuities or transition zones less than 10 km thick lying 150–250 km above the core–mantle boundary. Both wide- (Lay & Helmberger 1983; Weber 1993) and narrow-angle reflections (Schimmel & Paulssen 1996) are intermittently observed from this region, with coherent arrivals observed over distances typically less than 1000 km. Weber (1994) suggests that thin lamellae (of the order of 20 km in thickness and 2–3 per cent P- or S-velocity perturbation) of alternating high and low velocity may account for the observation of reflections from D″.

Evidence for ultra-low-velocity (greater than 10 per cent decrease) zones lying along some regions of the core–mantle boundary have been observed in core-grazing body waves (Garnero & Helmberger 1995; Sylvander *et al.* 1997; Wen & Helmberger 1998). These ultra-low-velocity zones have horizontal scale lengths of the order of several hundred kilometres and vertical scales of the order of several tens of kilometres. A model having lenses of high- and low-velocity material, elongated in the direction parallel to the core–mantle boundary, might be expected for horizontally lying remnants of descending slabs or for regions of strong horizontal convective flow. Such a model might also account for observations of short-period P waves far beyond the core shadow predicted by standard earth models (e.g. Bataille *et al.* 1990; Bataille & Lund 1996).

To test the importance of such a model to the excitation of $PKIKP$ precursors, the heterogeneity scale was taken to be 200–400 km in the horizontal direction and 10–20 km in the vertical direction. The horizontal scale is consistent with the coherency of D″ reflections, ultra-low-velocity zones, and waveguiding of short-period P waves that graze the

core–mantle boundary. The vertical scale is consistent with the maximum transition-zone thickness for reflections from the D″ region and thicknesses of ultra-low-velocity zones. In order to reproduce the power of observed precursors, a 1000-km-thick model of this type is found to have a perturbation of background *P* velocity of 8 per cent at 130° range and 30 per cent at 140° range. These high levels of perturbations are consistent with the high levels of perturbation found by Kendall & Silver (1998) to account for the transverse isotropy of *S* waves traversing a D″ model of disc-shaped inclusions. A perturbation as high as 30 per cent perturbation, however, would be observable as a large complex precursor signal on long-period and broad-band records, which is not observed (e.g. Fig. 1). These results suggest that if such heterogeneity exists, it must have velocity perturbations much smaller than 10 per cent, which would neither contribute significantly to the coda of the *PKIKP* precursor nor account for the transverse isotropy of *S* waves traversing the lowermost mantle.

Velocity perturbations as high as 3 per cent in a 250-km-thick layer of this type of model can contribute to the precursor coda at shorter range (130°) without affecting the precursor coda at longer range (140°). Fig. 5 shows the model constructed for testing, in which the D″ region is characterized by long horizontal and short vertical scale lengths, above which lies a mantle with isotropic heterogeneity. Synthetic seismograms (Fig. 6) show that such a model cannot fit the early precursor coda well. By 140° the apparent onset of observed precursor coda matches the minimum arrival time for scattering at the core–mantle boundary. This is not seen in the synthetics in Fig. 6. This problem is also illustrated in Fig. 9 by the

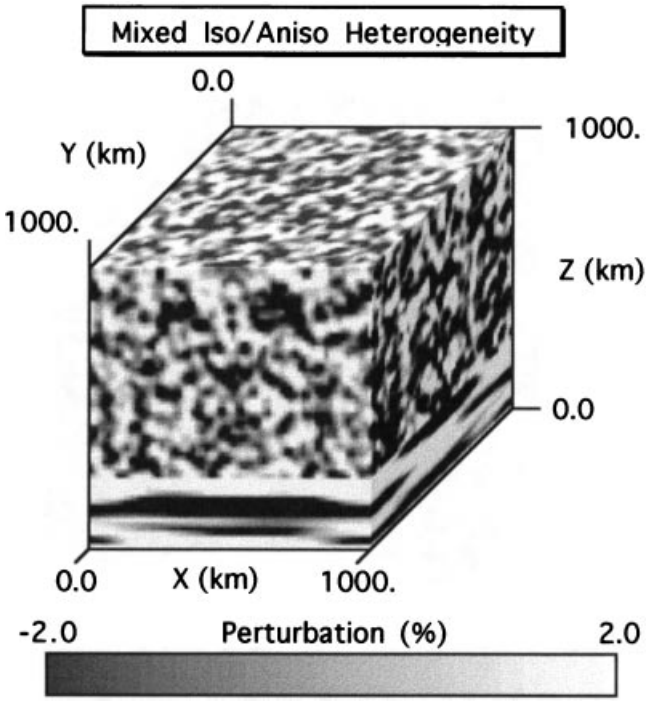

Figure 5. Model AHI.1000 of lower-mantle heterogeneity. A 250-km-thick D″ region has 2 per cent perturbation in *P* velocities with 200 km correlation lengths in the horizontal directions and 20 km correlation lengths in the vertical direction. Above D″ the heterogeneity distribution is isotropic with a 1 per cent perturbation in *P* velocity and a 20 km correlation length.

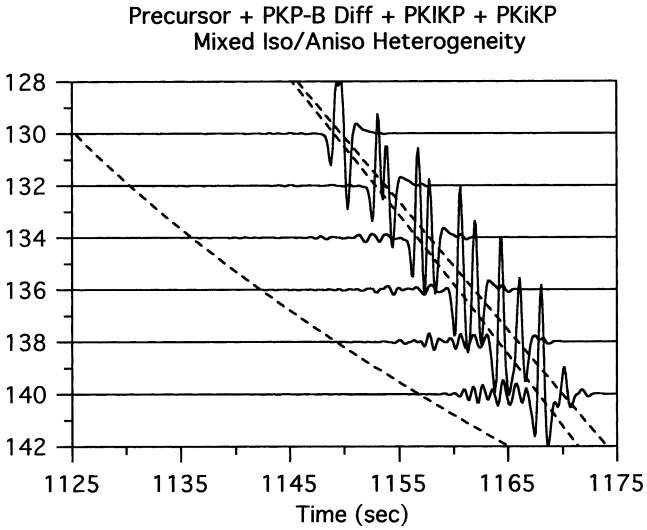

Figure 6. Synthetic record section of $PKIKP + PKiKP +$ scattered precursors for model AHI.1000 shown in Fig. 5. Instrument response and source spectrum are as in Fig. 3.

deterioration of the fit at earlier times to the stacked precursor envelopes measured by Hedlin *et al.* (1997). Such a model, however, may be made to fit observations if a more complex heterospectrum is assumed in D″. For example, an isotropic component having scale lengths of 20 km could be added to the anisotropic component in D″. Other successful models may be constructed by assuming different power laws in the horizontal versus vertical direction in D″. In this way, it might be possible simultaneously to satisfy *PKIKP* precursor data, wide- and narrow-angle reflections, and waveguiding of core-grazing body waves. The level of velocity perturbations in this type of model would be too small, however, to account for shear-wave splitting observed at wavelengths that are long compared to the vertical scale length. Two important conclusions result from testing this type of model: (1) the existence of a D″ heterospectral component having a much longer horizontal than vertical scale length does not appreciably affect the excitation of precursors to *PKIKP* for *P*-velocity perturbations as high as 3 per cent; and (2) an isotropic distribution of shorter-scale heterogeneity must continue to exist within D″ at a perturbation level similar to the region above D″.

2.2.2 *Large vertical scale/small horizontal scale*

Vertically stretched heterogeneity might possibly exist in regions of the lower mantle containing concentrations of plumes or slab remnants. 'Slab dumping' penetrating to and plumes originating from the core–mantle boundary occur in convection models that have a temperature dependence of viscosity (Steinbach & Yuen 1994). Although deep mantle plumes have yet to be seismically detected, evidence of near-vertically dipping slab remnants at mid-mantle depths is found in tomographic modelling (e.g. Grand 1994). These predictions and observations suggest the next model to be investigated: one in which the horizontal scale length is much shorter than the vertical scale length (Fig. 7).

Fig. 8 shows a synthetic record section for such a model that best fits coda shapes. Note that now the precursor onset

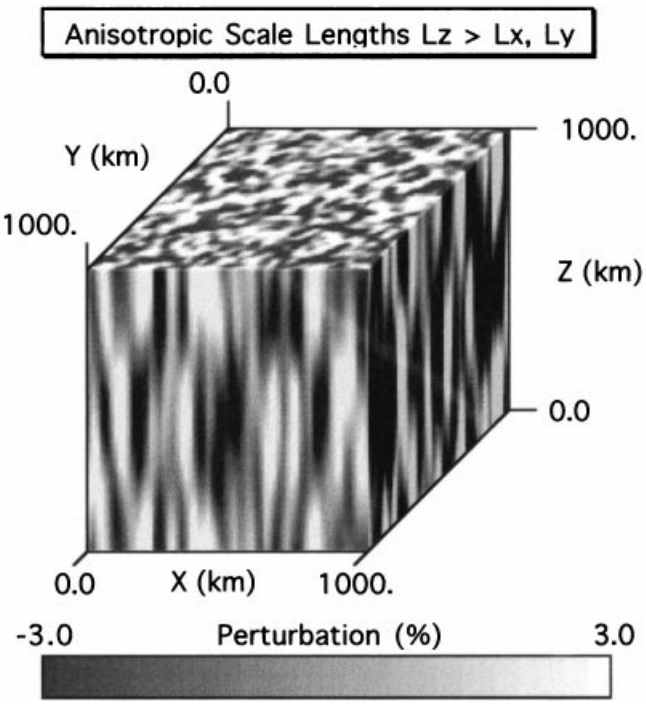

Figure 7. Model AV.1000 of heterogeneity in the lower mantle in which vertical scale lengths are much greater than horizontal scale lengths. A Gaussian autocorrelation is assumed with a longer correlation length in the vertical direction (200 km) than in the two orthogonal horizontal directions (20 km). Perturbation from the background *P* velocity is 3 per cent.

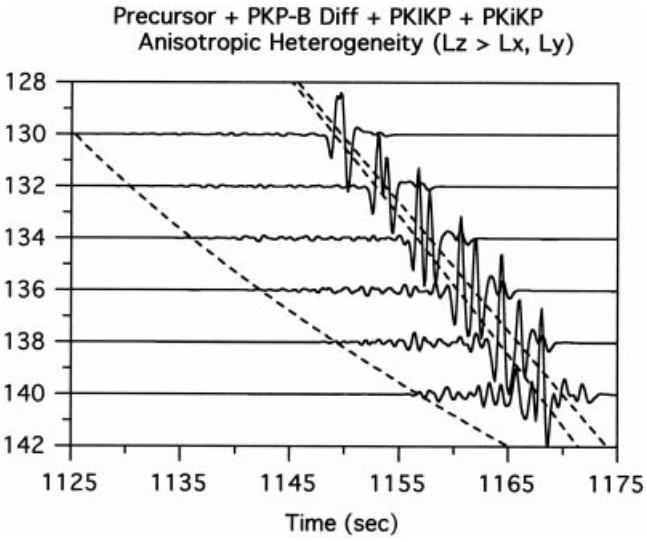

Figure 8. Synthetic record section for model AV.1000 shown in Fig. 7.

at 140° matches the minimum arrival time of waves scattered at the core–mantle boundary, similar to observations and results obtained for isotropic heterogeneity.

Fig. 9 compares the fits to observed coda shapes at 140° for models that have varying thicknesses of anisotropic and mixed anisotropic/isotropic heterogeneity above the core–mantle boundary. The best fit to the late coda for a model having long vertical/short horizontal scale lengths, as in the case of an isotropic distribution of scale lengths, is a model

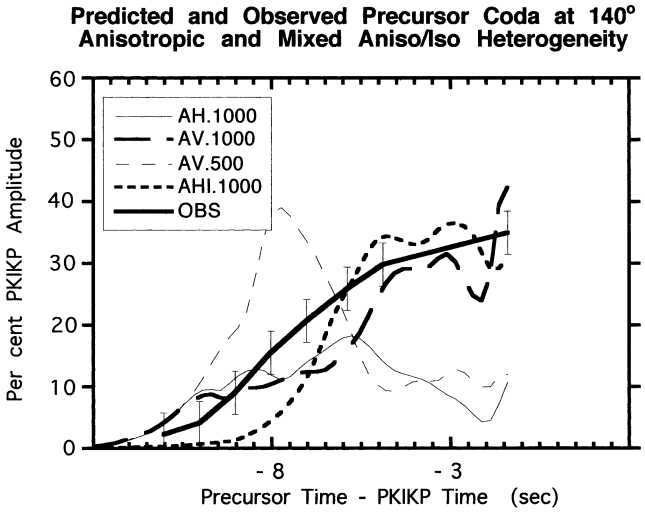

Figure 9. Predicted and observed scattered coda for different heights of heterogeneity with anisotropic and mixed anisotropic/isotropic distributions of scale lengths. Anisotropic heterogeneity has 200 km correlation lengths in the horizontal directions and 20 km in the vertical direction. Observed coda amplitudes at 140° are from Hedlin *et al.* (1997). Perturbations in *P* velocity and thicknesses of heterogeneity are 5.4 per cent and 1000 km for model AH.1000, 1.9 per cent and 500 km for model AV.500, and 1.8 per cent and 1000 km for model AV.1000. Model AHI.1000 consists of a 250-km-thick layer above the core–mantle boundary with an anisotropic heterospectrum with a 2 per cent *P*-velocity perturbation, followed by a 750-km-thick region with a 1 per cent *P* velocity perturbation.

that has heterogeneity extending 1000 km above the core–mantle boundary. At long wavelengths, this model is also equivalent to a transversely isotropic structure (e.g. Tandon & Weng 1984), with core-grazing *SV* now being faster rather than slower than core-grazing *SH* waves. For equal scale lengths in the two orthogonal horizontal directions as shown in Fig. 7, the *SH* and *SV* splitting will be independent of azimuth. This type of transverse isotropy (*SV* faster than *SH*), however, is relatively rare in observations of shear waves traversing the lower mantle. Pulliam & Sen (1998), for example, have found a such region of the central Pacific. Since the anisotropy they observe in this region vanishes for *S* waves bottoming above 150 km from the core–mantle boundary, it cannot be explained by vertically oriented inclusions extending up to 1000 km above the core–mantle boundary. Most observations find the reverse sense of transverse isotropy (*SH* faster than *SV*), concentrated in a 300-km-thick D″ layer (Vinnik *et al.* 1995; Kendall & Silver 1996), with little or no azimuthal anisotropy or transverse isotropy observed between D″ and the mantle below 650 km depth (Fouch & Fischer 1996).

3 PREFERRED MODELS

3.1 From precursor amplitude versus distance

Fig. 10 shows the best fits to observed peak precursor coda amplitudes for models having both isotropic and anisotropic scale lengths in the distance range 130°–140° in which *PKIKP* precursors are well observed. Gaussian autocorrelations are assumed in all models, but with different scale lengths in the three coordinate directions and a constant velocity

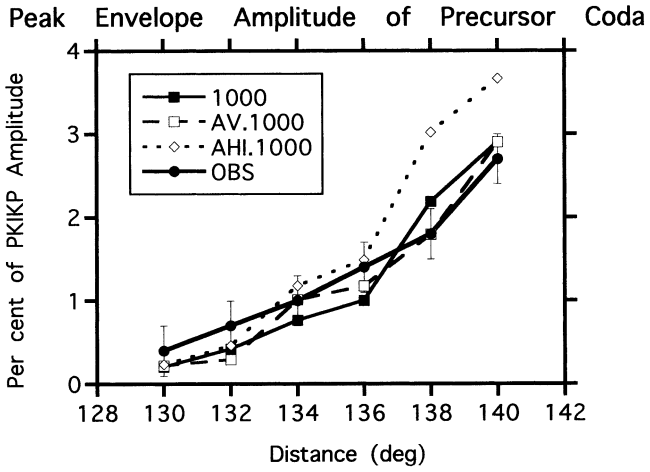

Figure 10. Peak envelope of precursor coda predicted by models I.1000, AV.1000 and AHI.1000 and measured (OBS) from the stacked data of Hedlin *et al.* (1997).

perturbation throughout the range of observations. Compared with the results of Hedlin *et al.* (1997), synthetic experiments in this paper do not find a strong range dependence of inferred velocity perturbation for a Gaussian scale length of 20 km. This difference in results may be due to a slightly lower dominant frequency (0.5–0.7 Hz) in the synthetics than in the data (1–1.3 Hz).

A good fit to these observations can be achieved with either an isotropic model of heterogeneity scale lengths (Fig. 2) or a model in which heterogeneity is stretched in the vertical direction (Fig. 7). Compared to the isotropic model (I.1000), the anisotropic model that has larger vertical than horizontal scale lengths (AV.1000) must have a higher intensity of perturbation to achieve a good fit. A 3 per cent perturbation is needed for a model that has a 20 km scale length in the horizontal directions and a 200 km scale length in the vertical direction. A mixed isotropic/anisotropic model that has larger horizontal scale lengths than vertical scale lengths in the D″ layer (AHI.1000) does not fit the amplitude growth rate of the precursors within the confidence limits established by Hedlin *et al.* from the standard deviations of stacked coda. As noted in the discussion of fits to coda shape, model AHI.1000 also does not fit the early part of the time window of stacked precursor coda data, nor does it predict the apparent onset of the coda as well as the isotropic model I.1000 or the anisotropic model AV.1000. It is possible, however, to construct a model similar to AHI.1000 which overcomes these problems, by adding an isotropic component of the heterospectrum in a 250-km-thick D″ layer. Thus, the results of experiments with models that have flat-lying disc-like heterogeneity in D″ simply show that the *PKIKP* precursor coda is insensitive to such structure.

3.2 From coda shapes

Although the stacked envelopes of precursor coda argue for the existence of heterogeneity throughout the lower 1000 km of the mantle, they may mask significant concentrations of heterogeneity at different depths and different regions. The coda shown in Fig. 1, for example, which was chosen at random to illustrate the frequency dependence and complexity of *PKP* waveforms in this distance range, is more consistent with heterogeneity concentrated in a 500-km-thick region above the core–mantle boundary than with a model in which heterogeneity continues at the same level of perturbation to 1000 km above the CMB. (Note how the precursor coda in Fig. 1 decays before the arrival of the CD branch rather than continuing at the same level of excitation as shown in the observed envelope in Fig. 4.) The variations in coda excitation as a function of time can be measured by the confidence limits shown in Hedlin *et al.* Because these confidence limits remain relatively uniform and small relative to the envelope amplitude throughout the time window considered, they suggest that concentrations of heterogeneity in narrow depth ranges and locations are not common. It is premature, however, to discount the possibility of strong regional variations in depth and level of perturbation of mantle heterogeneity without a much higher sampling of the lower mantle by observations of precursor coda. What *is* significant, however, is that the stacked precursor envelopes favour some level of small-scale heterogeneity throughout the lower mantle.

3.3 From precursor frequency content

3.3.1 Short period

The scale length of heterogeneity is known to affect the frequency content of scattered waves, showing particularly strong variations in frequency content in the transition from the Mie scattering domain (wavelengths of the order of or smaller than the heterogeneity scale length) to the Rayleigh scattering domain (wavelengths much larger than the scale length of heterogeneity). Using instruments that have a higher pass band than is currently common in DWWSN instruments, Ansell (1973) found that the precursor coda continues to have a higher frequency content than the direct *PKIKP*. In the frequency band of DWWSSN data (0.2–2 Hz), however, the high-frequency enrichment of the precursors is not obvious. Most DWWSSN waveforms have an essentially flat spectral ratio of precursors to *PKIKP* in the frequency band 0.9–3 Hz. Born scattering predicts the square of the spectral ratio to be proportional to the product of the fourth power of wavenumber times the wavenumber spectrum of heterogeneity (Chernov 1960). Thus, observations of precursor coda agree best with a power spectrum of heterogeneity that is proportional to the negative third to negative fourth power of wavenumber, resulting in a flat or slowly increasing spectral ratio with increasing frequency in the short-period band (0.1–1.5 Hz).

Fig. 11 compares the predictions for the spectral ratio of precursors to $PKIKP + PKiKP$ for several different models of heterogeneity spectra. Although a Gaussian heterogeneity spectrum may predict a precursor coda having a slow increase in frequency content relative to *PKIKP* with increasing frequency, it predicts a rapid decrease in frequency for wavenumbers greater than half the reciprocal correlation length. In Fig. 11 this rapid decrease in spectral ratio occurs around 0.5 Hz in a Gaussian model that has a correlation length of 20 km, suggesting that a correlation length of 10 km or less in a Gaussian model is needed to fit precursor observations around 1 Hz. A power spectrum of heterogeneity with a negative 5.3 power law (Bataille & Flatte 1988) would fail to predict the high-frequency enrichment of precursors observed by Ansell (1973). Bataille & Flatte also note that a power spectra

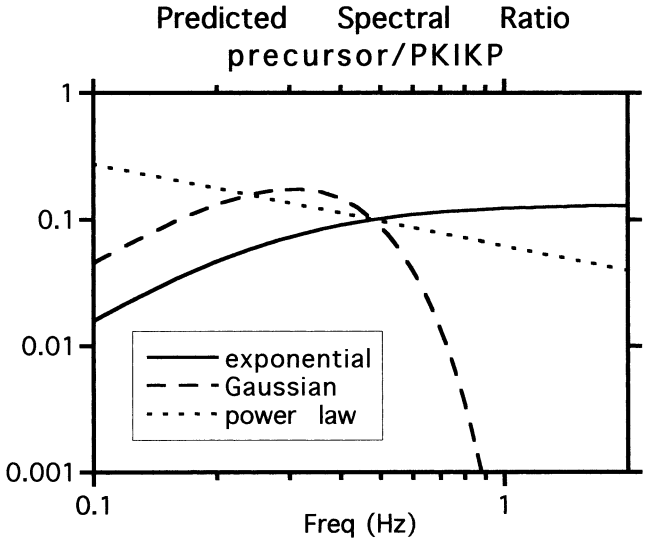

Figure 11. Predicted spectral ratio of precursor coda/*PKIKP* for different functional forms of the heterogeneity spectrum of the lower mantle. The abscissa in frequency corresponds to the wavenumber band 0.05–1 km^{-1}. Spectra are normalized to produce a ratio of 0.1 at wavenumber $k = 0.22$ km^{-1} ($f = 0.5$ Hz). The exponential spectrum assumes a scale length $a = 8$ km; the Gaussian spectrum, a scale length of 20 km; and the power law, a power of -5.3.

proportional to negative powers of wavenumbers cannot be extrapolated to lower wavenumbers without predicting too high a power of heterogeneity at the scale lengths resolved by global tomography.

3.3.2 *Broad band*

Because the precursor coda does not destroy the signature of the long-period diffraction from the B caustic (e.g. Fig. 1), broad-band data favour a power spectrum of heterogeneity that is either flat or slowly increasing with wavenumber in the band 0.05–0.5 km^{-1}. An exception to this general observation is the long-period data of Wen & Helmberger (1998), who find evidence for ultra-low-velocity zones in the western Pacific with *P*-velocity perturbations of 7 per cent or more in the lowermost 60–80 km. Most broad-band data, however, agree with the observations of Ansell (1973) in a higher frequency band, which are inconsistent with heterogeneity spectra proportional to a magnitude of negative power of wavenumber greater than 4.

Gaussian spectra having a single correlation length are too narrow in bandwidth to satisfy observations throughout the long- and short-period bands. Heterogeneity having an exponential autocorrelation, however, can easily satisfy observations of precursors over a broad range of wavenumbers. The power spectrum of the exponential autocorrelation behaves with wavenumber k like $1/(1 + Ck^2)^2$. Hence, the ratio of the power spectrum of the precursor to the power spectrum of *PKIKP* behaves like $k^4/(1 + Ck^2)^2$ and the ratio of the amplitude spectra like $k^2/(1 + Ck^2)$. For a single correlation length, an exponential autocorrelation predicts precursor excitation proportional to ω^2 at low frequencies and independent of frequency at high frequencies. At intermediate frequencies, corresponding to wavelengths roughly equal to the correlation length, the exponential autocorrelation predicts a weak increase in precursor excitation with frequency, consistent with observations over the 0.02–2 Hz band. This is the behaviour in the short-period band of the heterogeneity spectrum assumed in the modelling of Hedlin *et al.* (1997), who used an exponential autocorrelation with a scale length of 8 km for data with a dominant wavelength of 13 km.

3.3.3 *Anisotropy of scale lengths from frequency content*

In addition to the changes in frequency content induced by the functional form of the autocorrelation of heterogeneity, there are also are significant changes in frequency content between isotropic and anisotropic distributions of heterogeneity. Thus, it is possible to discriminate between isotropic and anisotropic distributions of mantle heterogeneity by carefully examining the frequency content of *PKIKP* precursors. Although experiments discussed in previous sections of this paper show that narrow-band data cannot discriminate between the isotropic and vertically stretched models of heterogeneity, broad-band modelling can demonstrate that vertically stretched heterogeneity is not a generally valid description of the lower mantle. Fig. 12, for example, shows broad-band synthetics for the three heterogeneous models of the lower mantle. Model AV.1000, with vertically elongated heterogeneity, predicts too high a level of precursor excitation in the long-period band to be consistent with broad-band data (e.g. Fig. 1). The isotropic distribution of scale lengths (I.1000) and the mixed anisotropic/isotropic model (AHI.1000) best fit precursor excitation observed in broad-band body waves. Although AHI.1000 seems to have an acceptable level of precursor excitation in a broad-band synthetic, it underpredicts the early high-frequency precursor coda observed in the short-period band. The isotropic model best predicts the behaviour of precursor coda, including both its shape and its frequency content, throughout the frequency band of teleseismic observations.

In summary, the broad-band behaviour of *PKIKP* precursors in the 0.02–2 Hz band is consistent with a heterospectrum of the lower mantle that slowly increases in power with increasing wavenumber in the band 0.05–0.5 km^{-1}, suggesting an exponential autocorrelation function having a scale length of the order of 10 km. It is not possible to satisfy

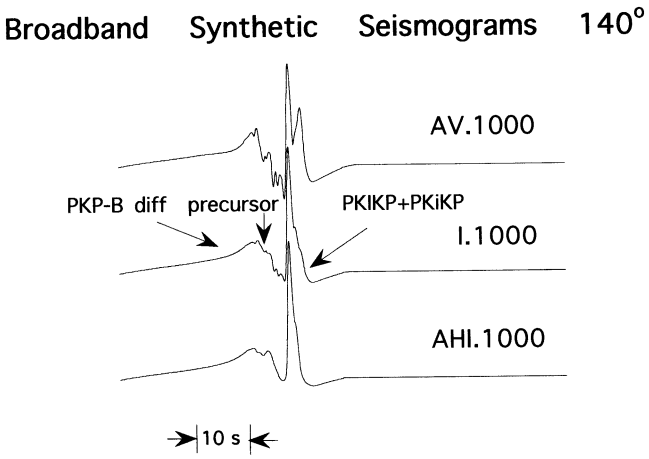

Figure 12. Broad-band synthetic seismograms for *PKP*-B diffraction + scattered precursor + *PKIKP* + *PKiKP* for three models of lower-mantle heterogeneity (AV.1000, I.1000 and AHI.1000).

this frequency dependence with heterogeneity models with any dominant anisotropy of scale lengths. The precursor frequency content of *PKIKP* precursors is inconsistent with a dominant fabric of vertically stretched, pencil-shaped heterogeneities. Precursors are insensitive, however, to distributions of horizontally stretched, disc-like heterogeneities. As much as 2–3 per cent *P*-velocity perturbation of this type may exist in a D″ layer as long as it is also accompanied by at least 1 per cent *P*-velocity perturbation at 50 km and smaller scale lengths, with an isotropic distribution of scale lengths. Beneath some regions, higher perturbations in heterogeneity that have both isotropic and anisotropic scale lengths may exist in the D″ depth range (Vidale & Hedlin 1998; Wen & Helmberger 1998).

3.4 From long-wavelength (SPO) anisotropy

Most observations of long-period *S* waves interacting with the lowermost mantle are consistent with transverse isotropy existing in a 150–200 km D″ layer. Lack of splitting originating in the lower mantle from observations of *SKS* waves (Fouch & Fischer 1996) requires either an isotropic or a transversely isotropic structure. The majority of observations of *S* waves bottoming in or steeply incident on the D″ region are consistent with transverse isotropy with a vertical axis of symmetry, making core-grazing *SH* faster than core-grazing *SV* (Kendall & Silver 1996; Lay & Young 1991; Matzel *et al.* 1996; Garnero & Lay 1997; Kendall & Silver 1998).

Although it is well known that the lower mantle is likely to be composed of minerals with significant intrinsic anisotropy (Stixrude 1998), it is difficult to construct a mechanism of lattice preferred orientation (LPO) of these minerals that results in primarily transverse isotropy (Kendall & Silver 1998). Karato *et al.* (1995), for example, have described a mechanism of superplasticity by which the intrinsically anisotropic minerals of the lower mantle would most probably be isotropic.

If LPO can be eliminated from consideration in the description of lower-mantle structure, then shape preferred orientation (SPO) anisotropy must be considered to explain the transverse isotropy seen in *S* waves traversing the lowermost mantle. *PKIKP* precursor data may permit the existence of some SPO anisotropy in the lower mantle, provided that the level of perturbation between horizontally oriented discs is 3 per cent or less. Kendall & Silver (1998), however, have shown that this level of heterogeneity is too weak to account for the observed traveltime differences of *SH* and *SV* waves travelling horizontally through the D″ region. Thus, some other mechanism must be found to account for the observed transverse isotropy of shear waves in D″—either the thin (hundreds of metres or less), horizontally lying discs of partial melt suggested by Kendall & Silver, or a lower-mantle petrology, mantle flow or remnant slab mineralogy consistent with LPO anisotropy at the pressure and temperature conditions of the core–mantle boundary.

4 DISCUSSION

4.1 Implications for mantle circulation

The current study is in agreement with the Hedlin *et al.* (1997) result that heterogeneity persists at undiminished intensity far above the core–mantle boundary. The great height of small-scale (10–50 km) heterogeneity above the core–mantle boundary is unlikely to be due to the circulation of products of a chemical reaction at the core–mantle boundary, which would tend to be denser than and negatively buoyant compared to the surrounding mantle (Kellogg & King 1993). Rather, the persistence of heterogeneity so far above the core–mantle boundary is suggestive of mantle-wide circulation (Olson & Kincaid 1991), possibly including slab penetration into the lower mantle.

4.2 The late time window of precursor coda

Inferences about the height of heterogeneity above the core–mantle boundary critically depend on the amplitude of the late precursor coda that arrives in a 5 s window just before the direct phases, primarily at distances near 140°. Given the significance of this result, some additional mechanisms were considered which could affect the amplitude of the late precursor coda.

One mechanism that could contribute to the coda in this time window is the effect of very long-wavelength heterogeneity not included in the laterally homogeneous model used as the reference earth for the synthesis of the direct phases. It is possible to show that large-scale heterogeneity allows scattering in the upper mantle, near the source and receiver, to contribute to the precursor coda in this late time window. The additional contribution comes from the scattering of inner-core phases, not usually considered in estimating precursor power because, in a laterally homogeneous reference earth model, the scattering of the inner-core phases contributes only to the energy arriving after the direct phase (e.g. Paper I). Ray-tracing tests were performed in models having the type of large-scale heterogeneity commonly resolved by global tomography. These tests found that only the last 1–1.5 s of the precursor coda may have some contributions from near-source or near-receiver scattering.

Another mechanism that may affect the late precursor coda is the source time function. Spatially extended or complex multiple sources may extend the precursor coda into the beginning of the waveform of the direct phase from the rupture initiation or the earliest multiple source. Surveys of DWWSSN recordings performed in the current study and in Paper I suggest that such effects are rare in the domain of the source sizes usually studied, which are characterized by fault lengths of the order of 10 km and simple source time functions of 2–3 s width.

4.3 Constraints on the power spectrum of heterogeneity

4.3.1 Lowermost 1000 km of the mantle.

Although global tomography cannot resolve the small scale lengths needed to explain *PKIKP* precursors, it finds that heterogeneity at much longer scale lengths, corresponding to wavenumber 0.003 km^{-1}, decreases below 1 per cent in the mid- and lower mantle (e.g. Woodward *et al.* 1994). If the heterogeneity of the lower mantle has an exponential autocorrelation, with a single dominant scale length of the order of 10 km, it can easily satisfy observations of heterogeneity across the wavenumber band of broad-band *PKIKP* precursors to the wavenumber band resolved by global tomography.

4.3.2 Changes in D″?

Although an increase in heterogeneity power in a thinner (150–250 km thick) zone in the lowermost mantle is not readily apparent in a global average of precursor coda, it is possible that an increase in heterogeneity with an anisotropic distribution of scale lengths may exist in such a zone and be undetectable in precursor coda if the distribution has large horizontal scale lengths relative to the vertical scale length. An alternative possibility is a significant increase in the standard deviation of the heterogeneity power in a D″ region, resulting in a well-developed layer of stronger heterogeneity in some regions and the absence of such a layer in other regions. Evidence of such behaviour is found in the western Pacific, which contains zones of more intense scattering (Vidale & Hedlin 1998) and ultra-low-velocity zones (Wen & Helmberger 1998) in the lowermost 50–100 km of the mantle. The work of Emmerich *et al.* (1993) suggests that further work may be needed in testing the effects of multiple scattering in regions where isotropic heterogeneity may be mistaken for anisotropic heterogeneity when velocity perturbations approach 5 per cent.

4.4 Signature of plumes and slabs in *PKIKP* precursors

Plume and slab structures, accompanied by strong velocity contrasts, may be detectable in the scattered *PKIKP* precursor coda. Model AV.1000, for example, might describe a lower mantle characterized by dense distributions of narrow conduits of the order of 10–30 km in diameter, which is in the range of scale lengths hypothesized for mantle plumes (Stacey & Loper 1983; Loper 1991). This type of structure would only be detectable in the short-period band if the level of *P*-velocity perturbation exceeds 3 per cent. Vertically dipping slab structures of the Caribbean anomaly type of 100–200 km thickness would be even less effective in generating observable *PKIKP* precursors. An exception to this prediction might be either deeply penetrating slabs that fragment or somehow transform into narrower tabular structures of the order of 10–30 km thickness or scattering from pre-existing thin-layered structures within the slab, such as the eclogite layer described by Gubbins & Snieder (1991) and Van der Hilst & Snieder (1996). If either thin, vertically dipping slab fragments or thin plumes existed in sufficient density in the lower mantle, then a transverse isotropy would be observed in the long-period shear waves that bottom in the lower mantle, with *SV* faster than *SH*. Since this sense of transverse isotropy is exceptional in observations, it can be concluded that such structures are also exceptional cases of mantle heterogeneity, a conclusion that is also in agreement with that reached from the frequency content of *PKIKP* precursors.

4.5 Melt inclusions

This paper has not specifically considered the effect of melt inclusions as a source of scattering that may contribute to precursor coda. Although it is difficult to find mechanisms leading to much partial melt in the lower mantle (Zerr *et al.* 1998), Kendall & Silver (1998) find that, if the melt resides in thin lenses, only a volume fraction of 0.01 per cent of partial melt is needed to explain the transverse isotropy of the lowermost mantle. Observations of ultra-low-velocity zones may also be evidence of some partial melt invasion in the lowermost 10–50 km of the mantle. If the boundaries of thin, horizontally oriented melt lenses, with scale lengths of 200 km or more, have sufficient topography on a scale length of 10–50 km, then they may also account for some of the *PKIKP* precursor coda. It is unlikely, however, that such structures persist globally to the height of 1000 km above the core–mantle boundary which is required to explain the shape of late precursor coda.

4.6 Scattering attenuation

The *P*-velocity perturbations required to explain the amplitude and frequency content of *PKIKP* precursors are generally not high enough to produce significant scattering or stratigraphic attenuation in body waves transmitted through the lower mantle. Numerical experiments (e.g. Cormier *et al.* 1998; Menke & Richards 1983), show that such attenuation does not have observable effects until perturbations in velocity exceed 5 per cent for path lengths of several hundred kilometres or more. If significant heterogeneity resides as laterally broad, horizontally lying discs in D″, it is possible that the 3 per cent heterogeneity in such structures permitted by observations of *PKIKP* precursors causes only a weakly observable amount of apparent attenuation in vertically incident body waves in D″. Thus, if future experiments reveal any significant body-wave attenuation in D″, this attenuation is more likely to be intrinsic attenuation than scattering attenuation. To date, however, few, if any, such experiments exist that are not complicated by the problem of separating the frequency dependence of spectral ratios caused by the effects of intrinsic attenuation from those caused by the effects of diffraction and tunnelling of core-grazing body waves.

5 CONCLUSIONS

5.1 Anisotropy of heterogeneity scale lengths

An anisotropic model of heterogeneity scale lengths having a longer vertical (200 km) than horizontal scale length (20 km) requires 3 per cent heterogeneity in the lower 1000 km of the mantle. The existence of such a model would be accompanied by the transverse isotropy of shear waves bottoming in the lower mantle, with *SV* being faster than *SH*. Such a model can be ruled out as a ubiquitous feature of the lower mantle, not only by the observed sense of transverse isotropy of *S* waves traversing the lower mantle, but also by the frequency content of long-period and broad-band precursors to *PKIKP*, which ride on top of the diffraction from the *PKP*-B caustic. Current shear-wave polarization data suggest that the existence of such a model in the lower mantle is a relatively rare occurrence, except in regions of the central Pacific (Pulliam & Sen 1998), which also exhibit a strong incoherence of relative *SH* and *SV* velocity over spatial areas with lateral dimensions of several degrees or less (Vinnik *et al.* 1995).

An anisotropic model of heterogeneity scale lengths with a much longer horizontal than vertical scale length does not significantly excite *PKIKP* precursors unless its *P*-velocity perturbation exceeds 10 per cent. Smaller perturbation levels in this type of model of 2–3 per cent, consistent with the perturbations needed to explain wide-angle reflections from D″ and waveguiding of short-period *P*, may indeed exist and even be required by mantle circulation at the core–mantle

boundary, yet remain largely undetectable in either the coda of *PKIKP* precursors or the transverse isotropy observed from *S* waves.

To account fully for the coda shape of *PKIKP* precursors, a small-scale (10–50 km) isotropic component of the heterospectrum must continue to exist in D″ to explain the apparent onset and early portion of *PKIKP* precursors. *P*-velocity fluctuations in this range of scale length must be of the order of 1 per cent to at least 800–1000 km above the core–mantle boundary to explain the stacked averages of late precursor coda.

5.2 Power spectrum of heterogeneity

The shape of the power spectrum of heterogeneity in the lower mantle must produce an amplitude spectrum of *PKIKP* precursors that is nearly white or slowly increasing with increasing frequency throughout the frequency band of broad-band body waves. This requirement, along with the requirements provided by an extrapolation of the heterogeneity spectrum resolved by global tomography, is satisfied by an exponential form of the autocorrelation of heterogeneity.

5.3 Topography of the core–mantle boundary

Topography by itself cannot explain *PKIKP* precursor coda shapes, particularly the late coda. The 20 km horizontal scale of 4 km high topography needed to explain the early portion of precursor coda would produce strong perturbations to *PcP* and *ScS* waveforms that are not seen in the data. The existence of a much smaller amount of topography at the core–mantle boundary (100–200 m height), with scale lengths of the order of 20 km, is consistent with the onset times of precursor coda, which at 140° tend to lie close to the predicted minimum arrival time for scattering at the core–mantle boundary.

ACKNOWLEDGMENTS

I thank Paul Earle, Michael Hedlin, Michael Kendall, Jay Pulliam, Peter Shearer and Lianxing Wen for preprints and reprints of their papers on *PKIKP* precursors and shear-wave anisotropy, and George Choy for broad-band deconvolved data. I also thank Nafi Toksoz and MIT-ERL's Center for Parallel Computation for use of their facilities for some of the computations. This research was supported by grant EAR 96–14525 from the National Science Foundation.

REFERENCES

Ansell, J.H., 1973. Precursors to PKP: seismic wave scattering in spectral data, *Geophys. J. R. astr. Soc.,* **35,** 487–489.

Bataille, K. & Flatte, S.M., 1988. Inhomogeneities near the core–mantle boundary inferred from short-period scattered PKP waves recorded at the Global Digital Seismograph Network, *J. geophys. Res.,* **93,** 15 057–15 064.

Bataille, K. & Lund, F., 1996. Strong scattering of short-period seismic waves by the core–mantle boundary and the P-diffracted wave, *Geophys. Res. Lett.,* **23,** 2413–2416.

Bataille, K., Wu, R.S. & Flatte, S.M., 1990. Inhomogeneities near the core–mantle boundary evidenced from scattered waves: a review, *Pageoph,* **132,** 151–173.

Chernov, L.A., 1960. *Wave Propagation in a Random Medium,* McGraw-Hill, New York.

Cleary, J.R. & Haddon, R.A.W., 1972. Seismic wave scattering near the core–mantle boundary: a new interpretation of precursors to PKP, *Nature,* **240,** 549–551.

Coates, R.T. & Charrette, E.E., 1993. A comparison of single scattering and finite difference synthetic seismograms in realizations of 2-D elastic random media, *Geophys. J. Int.,* **113,** 463–482.

Cormier, V.F., 1995. Time-domain modelling of *PKIKP* precursors for constraints on the heterogeneity in the lowermost mantle, *Geophys. J. Int.,* **121,** 725–736.

Cormier, V.F., Xu, L. & Choy, G.L., 1998. Seismic attenuation of the inner core: viscoelastic or stratigraphic, *Geophys. Res. Lett.,* **25,** 4019–4022.

Davis, J.P. & Henson, I.H., 1993. *User's Guide to Xgbm: an X-Windows System to Compute Gaussian Beam Synthetic Seismograms,* Rept TGAL-93–02, Teledyne-Geotech, Alexandria, VA.

Doornbos, D.J., 1976. Characteristics of lower mantle inhomogeneities from scattered waves, *Geophys. J. R. astr. Soc.,* **44,** 447–470.

Doornbos, D.J., 1988. Multiple scattering by topographic relief with application to the core–mantle boundary, *Geophys. J. Int.,* **92,** 465–478.

Dziewonski, A.M. & Anderson, D.L., 1981. Preliminary reference Earth model, *Phys. Earth planet. Inter.,* **25,** 3295–3314.

Emmerich, H., Zwielich, J. & Muller, G., 1993. Migration of synthetic seismograms for crustal structure with random heterogeneities, *Geophys. J. Int.,* **113,** 225–238.

Fouch, M.J. & Fischer, K.M., 1996. Mantle anisotropy beneath northwest Pacific subduction zones, *J. geophys. Res.,* **101,** 15 987–16 002.

Frankel, A. & Clayton, R.W., 1986. Finite difference simulations of seismic scattering; implications for the propagation of short-period seismic waves in the crust and models of crustal heterogeneity, *J. geophys. Res.,* **91,** 6465–6489.

Garnero, E.J. & Helmberger, D.V., 1995. A very slow basal layer underlying large scale low-velocity anomalies in the lower mantle beneath the Pacific: evidence from core-phases, *Phys. Earth. planet. Inter.,* **91,** 161–176.

Garnero, E.J. & Lay, T., 1997. Lateral variations in lowermost mantle shear wave anisotropy beneath north Pacific and Alaska, *J. geophys. Res.,* **102,** 8121–8135.

Grand, S.P., 1994. Mantle shear structure beneath the Americas and surrounding oceans, *J. geophys. Res.,* **99,** 11 591–11 621.

Gubbins, D. & Snieder, R., 1991. Dispersion of P waves in subducted lithosphere: evidence for an eclogite layer, *J. geophys. Res.,* **96,** 6321–6333.

Hedlin, M.A., Shearer, P.M. & Earle, P.S., 1997. Seismic evidence for small-scale heterogeneity throughout the Earth's mantle, *Nature,* **387,** 145–150.

Karato, S., Zhang, S. & Wenk, H.R., 1995. Superplasticity in Earth's lower mantle: evidence from seismic anisotropy and rock physics, *Science,* **270,** 458–461.

Kellogg, L.H. & King, S.D., 1993. Effect of mantle plumes on the growth of D′ by reaction between the core and mantle, *Geophys. Res. Lett.,* **20,** 379–382.

Kendall, J.M. & Shearer, P.M., 1994. Lateral variations in D″ thickness from long period shear wave data, *J. geophys. Res.,* **99,** 11 575–11 590.

Kendall, J.M. & Silver, P.G., 1996. Constraints from seismic anisotropy on the nature of the lowermost mantle, *Nature,* **381,** 408–412.

Kendall, J.M. & Silver, P.G., 1998. Investigating causes of D″ anisotropy, in *The Core–Mantle Boundary, Geodynamics,* Vol. 28, pp. 97–118, eds Gurnis, M., Wysession, M.E., Knittle, E. & Buffett, B.A., AGU, Washington.

Korneev, V.A. & Johnson, L.R., 1993. Scattering of elastic waves by a spherical inclusion—I. Theory and numerical results, *Geophys. J. Int.,* **115,** 230–250.

Lay, T. & Helmberger, D.V., 1983. A lower mantle S-wave triplication and the shear velocity structure of D″, *Geophys. J. R. astr. Soc.,* **75,** 799–837.

Lay, T. & Young, C.J., 1991. Analysis of SV waves in the core's penumbra, *Geophys. Res. Lett.,* **18,** 1373–1376.
Loper, D.E., 1991. Mantle plumes, *Tectonophysics,* **187,** 373–384.
Matzel, E., Sen, M. & Grand, S., 1996. Evidence for anisotropy in the D″ layer as inferred from the polarization of diffracted S waves, *Phys. Earth planet. Inter.,* **87,** 1–32.
Maupin, B., 1994. On the possibility of anisotropy in the D″ layer as inferred from the polarization of diffracted S waves, *Phys. Earth planet. Inter.,* **87,** 1–32.
Menke, W., 1986. Few 2–50 km corrugations on the core–mantle boundary, *Geophys. Res. Lett.,* **13,** 1501–1504.
Menke, W. & Richards, P.G., 1983. The apparent attenuation of a scattering medium, *Bull. seism. Soc. Am.,* **73,** 1005–1021.
Olson, P. & Kincaid, C., 1991. Experiments on the interaction of thermal convection and compositional layering at the base of the mantle, *J. geophys. Res.,* **96,** 4347–4354.
Pulliam, J. & Sen, M.K., 1998. Seismic anisotropy in the core–mantle transition zone, *Geophys. J. Int.,* **135,** 113–128.
Robertson, G.S. & Woodhouse, J.H., 1996. Ratio of relative S to P velocity heterogeneity in the lower mantle, *J. geophys. Res.,* **101,** 20 041–20 052.
Schimmel, M. & Paulssen, H., 1996. Steeply reflected ScSH precursors from the D″ region, *J. geophys. Res.,* **101,** 16 077–16 087.
Souriau, A. & Poupinet, G., 1993. Lateral variations in P velocity and attenuation in the D″ layer from diffracted P waves, *Phys. Earth planet. Inter.,* **84,** 227–234.
Stacey, F.D. & Loper, D.E., 1983. The thermal boundary-layer interpretation of D′ and its role as a plume source, *Phys. Earth planet. Inter.,* **33,** 45–55.
Steinbach, V. & Yuen, D.A., 1994. Effects of depth-dependent properties on the thermal anomalies in flush instabilities from phase transitions, *Phys. Earth planet. Inter.,* **85,** 65–183.
Stixrude, L., 1998. Elastic constants and anisotropy of $MgSiO_3$ perovskite, periclase, and SiO_2 at high pressure, in *The Core–Mantle Boundary, Geodynamics*, Vol. 28, pp. xx–96, eds Gurnis, M., Wysession, M.E., Knittle, E. & Buffett, B.A., AGU, Washington.
Sylvander, M. & Souriau, A., 1996. Mapping S-velocity heterogeneities in the D″ region from SmKS differential travel times, *Phys. Earth planet. Inter.,* **94,** 1–21.
Sylvander, M., Bruno, P. & Souriau, A., 1997. Seismic velocities at the core–mantle boundary inferred from P waves diffracted around the core, *Phys. Earth planet. Inter.,* **101,** 3–4.
Tandon, G.P. & Weng, G.J., 1984. The effect of aspect ratio of inclusions on the elastic properties of unidirectly aligned composites, *Polymer Composites,* **5,** 327–333.
Van der Hilst, R. & Snieder, R., 1996. High frequency precursors to P wave arrivals in New Zealand: implications for slab structure, *J. geophys. Res.,* **101,** 8473–8488.
Vidale, J.E. & Hedlin, M.A.H., 1998. Intense scattering at the core–mantle boundary north of Tonga: evidence for partial melt, *Nature,* **391,** 682.
Vinnik, L., Romanowicz, B., Le Stunff, Y. & Makeyeva, L., 1995. Seismic anisotropy and the D″ layer, *Geophys. Res. Lett.,* **22,** 1657, 1660.
Weber, M., 1993. *P*- and *S*-wave reflections from anomalies in the lowermost mantle, *Geophys. J. Int.,* **115,** 183–210.
Weber, M., 1994. Lamellae in D″? An alternative model for lower mantle anomalies, *Geophys. Res. Lett.,* **21,** 2531–2534.
Weber, M. & Davis, J.P., 1990. Evidence of laterally variable lower mantle structure from *P* and *S* waves., *Geophys. J. Int.,* **102,** 231–255.
Wen, L. & Helmberger, D.V., 1998. Ultra-low velocity zones near the core–mantle boundary from broadband PKP precursors, *Science,* **279,** 1701–1703.
Woodward, R.L., Dziewonski, A.M. & Peltier, W.R., 1994. Comparisons of seismic heterogeneity models and convective flow calculations, *Geophys. Res. Lett.,* **21,** 325–328.
Wysession, M.E., Okal, E.A. & Bina, C.R., 1992. The structure of the core–mantle boundary from diffracted waves, *J. geophys. Res.,* **97,** 8749–8764.
Wysession, M.E., Valenzuela, R.W., Zhu, A.-N. & Bartko, L., 1995. Investigating the base of the mantle using differential times, *Phys. Earth planet Inter.,* **92,** 67–84.
Zerr, A., Serghiou, G. & Boehler, R., 1998. On the solidus of the lower mantle and the stability of Mg-Si-Perovskite: new experimental results, *EOS, Trans. Am. geophys. Un.,* **79,** S214 (abstract).

APPENDIX A: COMPUTATIONAL NOTES

A1 Scattering assumptions

In Paper I, D″ scatterers were taken to be spheres to take advantage of a simple solution, valid in both the Rayleigh and Mie domains, for the scattered far-field radiation of a sphere developed by Korneev & Johnson (1993). Experiments in Paper I show that errors due to the assumption of Rayleigh scattering are bounded by 10 per cent in precursor amplitude for velocity perturbations approaching 10 per cent or more.

Another concern is the level of the velocity perturbation. Emmerich *et al.* (1993) show that when velocity perturbations are of the order of 5 per cent or more, the effects of multiple scattering become significant. Multiple scattering is omitted in both Paper I and the current paper because, for velocity perturbations of the order of 1 per cent, the effects of multiple scattering can be shown to be a second-order effect for the precursor problem. In the case of scattering by CMB topography, comparing the Rayleigh–Born approximation with an exact solution for multiple scattering, Doornbos (1988) showed that high vertical incidence angles minimize the effect of multiple scattering. Coates & Charrette (1993) compared finite difference modelling with the Rayleigh–Born approximation and found that the errors due to the assumption of single scattering increase in proportion to the length of time the wavefield propagates through a heterogeneous region and are greater for velocity than for impedance perturbations. For the high incidence angles and relatively short times of transit of precursor waves through a D″ scattering layer, multiple scattering can usually be neglected with small error even for velocity perturbations. Of some concern is the case of the anisotropic distribution of heterogeneity with much longer vertical than horizontal scale lengths. In this case, the neglect of multiple scattering can be larger due to the longer transit times at incidence angles nearly parallel to the vertical heterogeneities. The results of Coates & Charrette (1993), however, suggest that the errors would be greatest in traveltimes rather than the coda amplitudes that are compared with observations to discriminate between models of lower-mantle heterogeneity.

A2 Seismogram synthesis

Following Paper I, the spectral density of displacement for the scattered *P* wave is calculated by

$$\mathbf{U}_P(x_s, x_r) = \sqrt{\frac{\rho(x)\alpha(x)}{\rho(x_r)\alpha(x_r)}}\,\frac{\omega^2 \Delta V}{4\pi\alpha^2(x)} S'(\lambda_1, \lambda_2, \mu_1, \mu_2, \rho_1, \rho_1, \theta) \times U_P^{\mathrm{Ray}}(x_s, x)\mathbf{U}_P^{\mathrm{GB}}(x, x_r),$$

where x_s, x and x_r are source, scatterer and receiver coordinates; λ, μ, ρ and α are Lame's parameters, density, and *P* velocity,

respectively; ω is radian frequency; ΔV is a volume element of heterogeneity; U_P^{Ray} and $\mathbf{U}_P^{\mathrm{GB}}$ are defined in Paper I and are computed by dynamic ray tracing and beam summation, respectively. U_P^{Ray} has units of displacement spectral density and $\mathbf{U}_P^{\mathrm{GB}}$ has units of reciprocal length. S' is a non-dimensional scattering radiation factor given by $S' = Sq/j_1(q)$, where S and $q/j_1(q)$ are defined in Paper I.

Synthetic displacement spectra are obtained by summing the contributions from individual volume elements, ΔV, that discretize a continuously varying, 3-D, heterogeneous lower mantle. To ensure validity of Rayleigh scattering, the sizes of the linear dimensions of ΔV are taken to be a factor of 2 or smaller than the dominant incident wavelength of about 10 km (the ΔVs are cubes 4 km on a side). The synthetic spectra are filtered by a WWSSN-SP instrument response and a source spectrum (see Paper I) and inverse Fourier transformed to the time domain and added to the unscattered background field, which includes all direct *PKP* branches, including diffraction from the B caustic. Quantities for dynamic ray tracing, which are required for beam summation, are computed using the Xgbm subroutines of Davis & Henson (1993). U_P^{Ray} is computed from a function subroutine of geometric spreading and travel-times constructed from polynomial fits to amplitudes and times calculated by Xgbm. $\mathbf{U}_P^{\mathrm{GB}}$ is catalogued as a 33 Mbyte file of beam-summed seismograms calculated by Xgbm. $\mathbf{U}_P^{\mathrm{GB}}$ contains all inner- and outer-core *PKP* branches, for scatterers continuously distributed in the lower 1000 km of the mantle. Computation of the $\mathbf{U}_P^{\mathrm{GB}}$ is performed on a multiprocessor machine (MIT-ERL/Ncube Center for Parallel Computation).

A3 Model construction

Velocity perturbations are calculated by applying to three dimensions the methods described by Frankel & Clayton (1986) for two dimensions. In most of the calculations, a 3-D Gaussian autocorrelation function is assumed, of the form

$$A(x, y, z) = \exp\{-[(x/a)^2 + (y/b)^2 + (z/c)^2]\},$$

where a, b and c are correlation lengths in the x, y and z directions, respectively. The wavenumber power spectrum of heterogeneity is given by the 3-D Fourier transform of $A(x, y, z)$,

$$\hat{A}(k_x, k_y, k_z) = \pi^{3/2} abc \exp\{-[(ak_x)^2 + (bk_y)^2 + (ck_z)^2]/4\}.$$

Test calculations were also made with spectra of the power-law type recommended by Bataille & Flatte (1988):

$$\hat{A}(k_x, k_y, k_z) = \phi_0 (k_x^2 + k_y^2 + k_z^2)^{p/2},$$

where ϕ_0 is a constant and p is a power estimated by Bataille & Flatte (1988) from fits to peak precursor coda amplitudes in the 130°–140° range. To avoid spatial aliasing and renormalization due to discretization of the medium and truncation of the spectrum, the power-law-type spectrum is filtered by a Butterworth bandpass with corners at $|k| = 2\pi/70$ and $|k| = 2\pi/10$, corresponding to the wavenumber band observed by Bataille & Flatte (1988). Comparisons of results with the Gaussian power spectrum and the power-law spectrum show that the short-period pass band is too narrow to discriminate easily between the two representations (e.g. see results for models I.250 and I.250P in Fig. 4). A broad-band recording, as noted in Sections 3 and 4, favours power laws with p between –3 and –4, which can also be achieved with exponential autocorrelations with a single scale length of the order of 10 km.

The velocity perturbation in wavenumber space is constructed by multiplying a white spectrum with a random phase at discrete wavenumbers in a 3-D grid by the square root of $\hat{A}$. In the space domain, the heterogeneous model is then found by performing an inverse 3-D FFT to space, normalizing the result by the standard deviation, and multiplying by the desired value of $\delta\alpha/\alpha$. Although Bataille & Flatte (1988) show that the scattered precursors to *PKIKP* are nearly insensitive to variations in density and shear velocity, a scaling is assumed in which $\Delta\rho/\rho = 0.1\delta\alpha/\alpha$ and $\delta\beta/\beta = 1.5\delta\alpha/\alpha$. [Robertson & Woodhouse (1996) find $\delta\beta/\beta = 2\delta\alpha/\alpha$ to be an appropriate scaling for the lower mantle.]

All calculations are performed in a spherical earth, but with velocity perturbations specified on a Cartesian grid. Perturbations were specified on a 1000 km × 1000 km × 1000 km grid of the type shown in Figs 2, 5 and 7, sampled at 4 km intervals. The X-axis is taken in the plane containing the source, receiver and centre of the Earth, tangent to the core–mantle boundary with an origin 4° shorter than the B caustic distance for a scatterer at the core–mantle boundary. Radiation from discrete scatterers located at all positions in three dimensions is summed until arrival times are 2 s later than the unscattered *PKIKP* phase. The heterogeneous models are assumed to be periodic to obtain velocity perturbation values outside the bounds of the 1000 km^3 grid.